Journal of Power Sources 205 (2012) 402–407

Contents lists available at SciVerse ScienceDirect

Journal of Power Sources

journal homepage: www.elsevier.com/locate/jpowsour

Graphite and $LiCo_{1/3}Mn_{1/3}Ni_{1/3}O_2$ electrodes with piperidinium ionic liquid and lithium bis(fluorosulfonyl)imide for Li-ion batteries

Jakub Reiter[a,*], Martina Nádherná[b], Robert Dominko[c,d]

[a] Institute of Inorganic Chemistry of the ASCR, v.v.i., 250 68 Řež near Prague, Czech Republic
[b] Department of Analytical Chemistry, Faculty of Science, Charles University in Prague, Albertov 2030, 128 40 Prague 2, Czech Republic
[c] National Institute of Chemistry, Hajdrihova 19, SI-1000 Ljubljana, Slovenia
[d] CO-NOT Centre of Excellence, Hajdrihova 19, SI-1000 Ljubljana, Slovenia

ARTICLE INFO

Article history:
Received 16 August 2011
Received in revised form
23 November 2011
Accepted 1 January 2012
Available online 9 January 2012

Keywords:
Graphite
Lithium cobalt manganese nickel oxide
Ionic liquid
Piperidinium
Bis(fluorosulfonyl)imide
Solid electrolyte interface

ABSTRACT

A new ionic liquid-based electrolyte for lithium batteries operating at an elevated temperature of 55 °C was prepared by combining N-methyl-N-propylpiperidinium bis(trifluoromethanesulfonyl)imide (PP_{13}TFSI) and lithium bis(fluorosulfonyl)imide (LiFSI). The electrolyte does not contain volatile organic components and is thermally stable (up to 285 °C) and ionically conductive (2.6 mS cm^{-1} at 55 °C). The 0.7m LiFSI–PP_{13}TFSI electrolyte has been shown to work effectively with a graphite anode due to the ability of the FSI anions to create a stable solid electrolyte interface on graphite. A discharge capacity of 340–345 mAh g^{-1} was achieved at C/10 rate with a coulombic efficiency of 97–98%. The electrolyte is also compatible with $LiCo_{1/3}Mn_{1/3}Ni_{1/3}O_2$ (NMC) cathode material. At the C/10 rate, we achieved a discharge capacity of 160 mAh g^{-1}. The coulombic efficiency remains high above 99%.

1. Introduction

Room temperature ionic liquids (RTILs, ILs) with aliphatic nitrogen cations attract the attention of many scientists dealing with lithium-ion batteries. This interest is caused by their unique properties: wide liquid range, a wide electrochemical stability window, good ionic conductivity, negligible volatility, non-flammability, etc. [1,2]. The substitution of a common, organic carbonate-based electrolyte with an IL-based electrolyte leads to a significant improvement in system safety and the reduction of environmental risks and negative impacts on human health.

Quaternary aliphatic or alicyclic cations belong to the most electrochemical stable organic moieties [3,4]. Many papers have been published on the compatibility of various cathodic materials, such as $LiFePO_4$ [5–8], Li_2FeSiO_4 [9], $LiMn_2O_4$ [10,11], $LiNi_{0.5}Mn_{1.5}O_4$ [12–14], $Li_xTi_yMn_{1-y}O_2$ [15], and $LiCoO_2$ [16–23].

Despite the outstanding stability of some ionic liquids at low potentials, graphite is not compatible with most ILs due to the irreversible electrochemical reduction of imidazolium cations on graphite or due to the intercalation of the organic cations such as $TMHA^+$, PYR_{13}^+, PYR_{14}^+ and PP_{13}^+ between the graphene layers observed by Zheng [24], Sun [25] and Aurbach [26]. The solution is to use either organic additives [25,27,28] or in using bis(fluorosulfonyl)imide FSI^- anion as an inherent part of the electrolyte [29–31]. However, the FSI-based ionic liquids show a lower electrochemical stability window than the TFSI analogues [29,32], slightly worse safety properties with charged electrode materials [33] and a higher production cost. These handicaps can be overcome by using electrolytes with a lower content of FSI^- anion such as PYR_{14}TFSI–PYR_{13}FSI–LiTFSI [30] or PYR_{14}TFSI–LiFSI [34].

Another advantage of ionic liquids is in their higher chemical stability with charged (delithiated) layered oxides. Egashira et al. showed the thermal stability of cyano-substituted quaternary ammonium ionic liquids with $Li_{0.46}CoO_2$ electrode up to 260 °C, 50 °C higher than conventional carbonate-based electrolytes [21]. A similar improvement was observed by Wang et al. with various electrolytes and Li_1Si, $Li_7Ti_4O_{12}$ and $Li_{0.45}CoO_2$ electrode materials investigated using accelerating rate calorimetry [33]. Aurbach and co-workers reported that the addition of 10% of TFSI-based ionic liquid to a conventional carbonate-based electrolyte considerably improves the thermal stability of the Li/$LiCoO_2$ system [35]. However, the stability of particular electrolyte requires a thorough check

* Corresponding author. Current address: Münster Electrochemical Energy Technology, Institute of Physical Chemistry, Westfälische Wilhelms-Universität Münster, Corrensstr. 46, 48149 Münster, Germany. Tel.: +49 251 8336777; fax: +49 251 8336032.
E-mail address: jakub.reiter@uni-muenster.de (J. Reiter).

0378-7753/$ – see front matter © 2012 Elsevier B.V. All rights reserved.
doi:10.1016/j.jpowsour.2012.01.003

using accelerating rate calorimetry, thermal analysis and flammability tests [33,36].

In this work, we evaluate the compatibility and electrochemical performance of an electrolyte based on 1-methyl-1-propylpiperidinium bis(trifluoromethanesulfonyl)imide (PP_{13}TFSI) and lithium bis(fluorosulfonyl)imide (LiFSI). Highly crystalline KS6L graphite was used for the anode material, whilst lithium cobalt manganese nickel oxide $LiCo_{1/3}Mn_{1/3}Ni_{1/3}O_2$ (NMC) was used as a representative of the cathode material. Our focus is the optimisation of the ionic liquid-based electrolyte compatible with graphite and NMC at 55 °C without the presence of any organic additive.

PP_{13}TFSI exhibits high electrochemical stability with a typical accessible electrochemical window on inert materials (gold, platinum, glassy carbon) exceeding 5 V. Xiang [37] presented the anodic stability up to 5.5 V on stainless steel and Sakaebe [16] showed a broad window on glassy carbon from −3.3 to 2.5 V vs. Fc/Fc^+, which is a significantly higher window than for, i.e. imidazolium-based ILs. The cathodic stability of PP_{13}TFSI allows reversible lithium plating and stripping on platinum as was shown by Sun in the case of LiTFSI–PP_{13}TFSI electrolyte [25]. The electrochemical properties of LiFSI have been thoroughly studied in organic carbonates [38,39] as well as in ionic liquids [40]. All papers present excellent properties of LiFSI, such as ionic conductivity, high cathodic and anodic stability and also compatibility with an aluminium current collector.

2. Experimental

2.1. The synthesis of ionic liquids, the preparation of electrolytes

The method of preparation is based on a two-step synthesis, with bromide being prepared by direct alkylation of N-methylpiperidine and then substituted with bis(trifluoromethanesulfonyl)imide in an aqueous solution. 1-Bromopropane (>96%) and N-methylpiperidine (>99%) were purchased from Sigma–Aldrich, LiTFSI (>99%; battery grade) from Ferro (USA), all being used as received.

A total of 62.0 g (0.5 mol) of 1-bromopropane was mixed with 49.6 g (0.5 mol) of N-methylpiperidine in a flask with a reflux condenser. The mixture was stirred at 50 °C for 6 h to give a slightly yellow solid. This yellow impurity was removed by hot acetonitrile under rigorous mixing at 80 °C. White $PP_{13}Br$ was filtered off, rinsed with acetonitrile and dried overnight at 65 °C under vacuum to give a white solid (85 g; 76% yield). Contrary to pyrrolidinium-based bromides ($PYR_{13}Br$, $PYR_{14}Br$), $PP_{13}Br$ is poorly soluble in acetonitrile.

The substitution of bromide anion by $TFSI^-$ was performed in water, where PP_{13}TFSI is not soluble and forms hydrophobic globules at the bottom of the flask. The amount of 71.77 g (0.25 mol) of LiTFSI in 120 ml of water was added to a solution of 55.54 g (0.25 mol) $PP_{13}Br$ in 100 ml of distilled water and stirred overnight at 50 °C. The arising phase of colourless PYR_{13}TFSI was removed and washed 4 times with 100 ml portions of distilled water and than 2 times with 100 ml portions of deionised water to remove the LiBr. The absence of bromide anions was confirmed using the test with $AgNO_3$. The remaining water was evaporated under vacuum at 55 °C at a rotary evaporator.

PP_{13}TFSI was purified by treatment with alumina (Brockmann acidic I, Sigma–Aldrich) and active carbon (Darco G60, Sigma–Aldrich) in acetone (HPLC grade, Merck). After purification, the remaining acetone was evaporated under vacuum and pure PP_{13}TFSI was dried at 15 Pa and 100 °C for 24 h before being stored in a dry argon-filled glove box ($[H_2O] < 1$ ppm; MBraun, USA). Yield: 89 g of colourless liquid (84%).

The purity of dry ionic liquids was confirmed by NMR measured using a Varian MERCURY 400 High Resolution NMR Spectrometer: PP_{13}TFSI—δH (400 MHz, $CDCl_3$, ppm): 1.06 (3 H, t, $CH_2CH_2CH_3$), 1.6–1.9 (8 H, br, $CH_2CH_2CH_3$ and ring), 3.07 (3 H, s, CH_3), 3.28 (2H, t, $CH_2CH_2CH_3$), 3.38 (4H, br, ring).

Lithium bis(fluorosulfonyl)imide (LiFSI) was synthesised according to the procedure published by Beran and Příhoda [41,42] and dried at 15 Pa and 65 °C for 20 h before being stored in the glove box. IR and NMR spectroscopy and IEC showed no presence of organic impurities and inorganic ions. The electrolyte, 0.7m LiFSI in PP_{13}TFSI was prepared by dissolving the salt in PP_{13}TFSI in the glove box at an ambient temperature. The water content was checked by the Karl Fischer titration and is below 3.5 ppm. The concentration is expressed in molality (moles of the salt in 1 kg of solvent).

2.2. The preparation of the electrodes and electrochemical tests

Anode electrode composites of graphite–carbon black (CB)–PVDF samples were prepared using KS6L graphite (Timcal, Switzerland). The composite consisted of 85 wt.% of graphite, 10 wt.% of carbon black (C-nergy™ Super C65, Timcal) and 5 wt.% of PVDF (M_n 534,000, Sigma–Aldrich) as a binder. The resulting slurry in 1-methyl-2-pyrrolidone (Sigma–Aldrich) was cast onto a circular Cu foil with a diameter of 12 mm (1.13 cm^2) with a loading of 0.8–1.1 mg cm^{-2}.

The cathode electrode composites consisted of 80 wt.% of $LiCo_{1/3}Mn_{1/3}Ni_{1/3}O_2$, 10 wt.% carbon black (C-nergy™ Super C65, Timcal) and 10% of PVDF as a binder. The resulting slurry in 1-methyl-2-pyrrolidone (Sigma–Aldrich) was cast on a circular Al foil with a diameter of 12 mm (1.13 cm^2) with a loading of 5 mg cm^{-2}.

All the electrodes were dried in vacuum at 90 °C for at least 12 h prior to use.

2.3. Methods and equipment for electrolyte characterisation

The potentio-galvanostats PGSTAT 10, 20 and 30 (Eco Chemie, The Netherlands) were used for electrochemical measurements. The electrochemical properties were measured in ECC standard cells (EL-Cell, Germany) by using a Celgard® 2320 as a separator and a lithium foil as counter and reference electrodes. The experimental temperature for all the voltammetric and galvanostatic measurements was 55 °C.

The galvanostatic measurements with the graphite electrodes were performed with a current density corresponding to C/10 in the potential range from 2 V to 0 V vs. Li/Li^+. The slow scan-rate cyclic voltammetry was performed at 0.1 mV s^{-1} in the potential range from 2 to 0 V vs. Li/Li^+.

The galvanostatic measurements with the NMC electrodes were performed with the current densities C/10 in the potential range from 2.5 to 4.3 V vs. Li/Li^+.

Temperature dependent conductivity measurements were performed in the temperature range from 0 to 100 °C using a Ministat 125-cc circulating bath (the precision of the temperature ± 0.1 °C, Huber, Germany) and a conductivity cell (Jenway, platinum electrodes, cell constant $S = 1.00 \pm 0.01$). Using the FRA-2 module of the PGSTAT 30 potentiostat, a single potential impedance spectrum was measured in the frequency range from 10 kHz to 100 Hz. The obtained spectrum was analysed using the EcoChemie Autolab software producing the value of electrolyte resistivity.

The TGA–DTA measurement was performed in an argon flow at the heating rate of 5 °C min^{-1} with a Simultaneous Thermal Analysis Netzsch STA 409 (Germany).

3. Results and discussion

3.1. The thermal stability of the ionic liquid electrolytes

The key safety advantage of ionic liquids is their non-flammability and high thermal stability. The classical, molecular

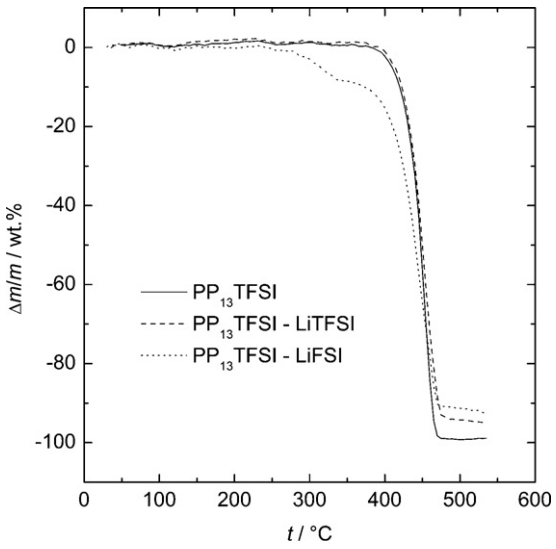

Fig. 1. TGA curves for a neat $PP_{13}TFSI$ and 0.7m LiFSI solution in $PP_{13}TFSI$ (5 °C min^{-1} heating rate, temperature range 30–550 °C; argon atmosphere).

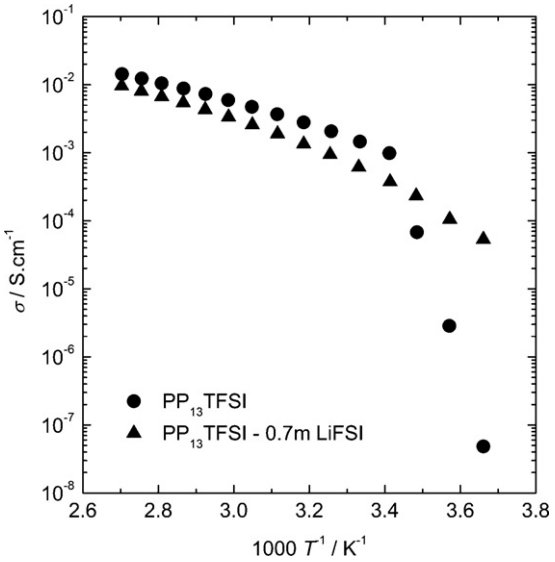

Fig. 2. Arrhenius plot for a neat $PP_{13}TFSI$ and 0.7m LiFSI solution in $PP_{13}TFSI$ (temperature range 0–100 °C).

solvent-based electrolytes show a decrease in weight due to solvent evaporation and combustion at increased temperatures. In contrast to the majority of organic compounds, ionic liquids remain stable up to temperatures above 350 °C and they usually decompose in one step by carbonisation rather than exothermic oxidation, which is particularly valid for ionic liquids with perfluorinated anions [36].

The thermal stabilities of $PP_{13}TFSI$ ionic liquid with LiTFSI or LiFSI were tested in an argon atmosphere up to 535 °C at a heating rate of 5 °C min^{-1}. Fig. 1 presents the decomposition curves. All the samples have only minimal weight loss (less than 0.2 wt.%) below 250 °C. The high thermal stability of $PP_{13}TFSI$ and LiTFSI–$PP_{13}TFSI$ samples, up to 395–400 °C, is in agreement with the results observed by Sun and Dai [25] and Xiang et al. [37].

A noticeable loss (above 1 wt.%) was observed above 285 °C in the case of LiFSI–$PP_{13}TFSI$ electrolyte, whilst the neat $PP_{13}TFSI$ remains stable up to 395 °C. In all cases, a single-step decomposition reaction occurs at rather high temperatures of 400–500 °C.

Ionic liquids with FSI anion are thermally less stable than the TFSI analogues. The present SO_2F group is more reactive towards water than SO_2CF_3, particularly at elevated temperatures and in the presence of water traces. Lithium bis(fluorosulfonyl)imide itself is thermally stable up to 200–300 °C (Ref. [38]), which is higher than for $LiPF_6$ (107 °C), but lower than for LiTFSI (350 °C), but it degrades rapidly above 120 °C in the presence of water traces and is strongly hydroscopic. A possible mechanism for the decomposition of LiFSI could be that heating promotes breakage of the sulphur—nitrogen bond in the anion to form a radical $FSO_2^{\bullet}$. Thermal behaviour of LiFSI–$PP_{13}TFSI$ system is more complex. When the electrolyte contains both the FSI^- and $TFSI^-$ ions, the Li^+ ions show preference to form $Li_x(FSI)_y$ complex. In the presence of water is the complex decomposed at lower temperatures that one would expect from the TGA curves of neat LiFSI and $PP_{13}TFSI$.

The LiFSI–$PYR_{14}FSI$ and LiFSI–$PYR_{13}FSI$ electrolyte studied by Paillard [32] and Zhou [40] showed partial decomposition already above 100 °C and even at 75 °C using isothermal TGA. The main single decomposition step, however, occurred at ca. 300 °C. This is consistent with our observation of a small decomposition wave in the region from 285 to 400 °C in the LiFSI–$PP_{13}TFSI$ electrolyte (see Fig. 1), where the FSI^- anion content is lower. The results of the TGA analysis support the intention of designing electrolyte with lower content of the FSI anion.

3.2. The conductivity of ionic liquid electrolytes

The conductivity of IL had been regarded as an important property for its application as a solvent for the electrolyte in various electrochemical devices, and it could be mainly governed by the molecular weight, density and viscosity of IL.

The change of ionic conductivity with temperature was measured in the region from 0 to 100 °C and is shown in Fig. 2. At temperatures above 15 °C, the conductivity of the electrolyte is lower that the conductivity of neat $PP_{13}TFSI$. As expected, the bulk conductivity of the lithium salt solution in IL is lower and viscosity is higher than that for neat $PP_{13}TFSI$. The equilibrium

$$(PP_{13}{}^{+})_{dissoc} + (TFSI^{-})_{dissoc} \leftrightarrow (PP_{13}\cdots TFSI^{-})_{assoc} \quad (1)$$

is shifted to the right by addition of lithium salt. Increased ion–ion pairs or aggregates than causes a decrease of conductivity. Similarly to our previously studied LiFSI–$PYR_{14}TFSI$ and LiTFSI–$PYR_{14}TFSI$ electrolytes [9,34], presence of a different anion (FSI^- or PF_6^-) in TFSI ionic liquid is favourable, because the conductivity drop is not so deep. Generally, the ionic liquids and their lithium salt solutions show a lower conductivity that the conventional carbonate-based electrolytes, especially at low temperatures. This disadvantage can be overcome by the addition of organic solvents [37,43,44], using ionic liquid mixtures or by elevation of the operation temperature [9,33], that shift the equilibrium described above to the left.

Below 15 °C, a dramatic decrease in conductivity of the neat $PP_{13}TFSI$ is caused by its solidification, whilst the electrolyte solution (LiFSI–$PP_{13}TFSI$) retains a reasonable conductivity of 10^{-4} S cm^{-1} even at 0 °C (see Fig. 2), possibly due to ion confusion effect [45] or to formation of a supercooled solution. At 55 °C, the conductivity of neat $PP_{13}TFSI$ and 0.7m LiFSI in $PP_{13}TFSI$ is 4.7 and 2.6 mS cm^{-1}, respectively.

The temperature dependence of conductivity for neat $PP_{13}TFSI$ and LiFSI–$PP_{13}TFSI$ electrolyte is probably best described using the Vogel–Tamman–Fulcher model [46] over the temperature range studied. The VTF equation is believed to describe more accurately the σ–T behaviour of systems containing high concentrations of ions (i.e. greater than 0.1 M). The apparent activation energy for the studied systems together with the confidence interval of the VTF fit is summarised in Table 1. Compared to the previously studied LiFSI–$PYR_{14}TFSI$ and LiTFSI–$PYR_{14}TFSI$ electrolytes, one can see

Table 1
Specific conductivities (at 20 and 55 °C), apparent activation energy E_A from the fit by the VTF equation and the start decomposition temperatures (T_{dec}) determined by the TGA of the studied electrolytes. For comparison, data about $PYR_{14}TFSI$ and $PYR_{14}TFSI$–0.7m LiFSI electrolyte are shown from [34].

Electrolyte	σ (20 °C) (mS cm^{-1})	σ (55 °C) (mS cm^{-1})	E_A (kJ mol^{-1})	T_0 (°C)	T_{dec} (°C)
$PP_{13}TFSI$	1.0	4.7	6.7	−96	395
$PP_{13}TFSI$–0.7m LiFSI	0.4	2.6	6.3	−78	285
$PYR_{14}TFSI$	2.1	7.3	6.9	−113	385
$PYR_{14}TFSI$–0.7m LiFSI	1.5	5.7	6.8	−103	205

lower conductivities of the electrolyte based on piperidinium (see Table 1).

3.3. Cyclic voltammetry on graphite

The electrochemical behaviour of the graphite composite electrode in neat $PP_{13}TFSI$ and two electrolytes LiTFSI–$PP_{13}TFSI$ and LiFSI–$PP_{13}TFSI$ was investigated using cyclic voltammetry. The voltammograms shown in Fig. 3 were obtained between 2.0 and 0 V vs. Li/Li$^+$ at a scan rate of 0.1 mV s^{-1}. The broad cathodic peak between 0.8 and 0.4 V can be attributed to the intercalation of PP_{13}^+ cations into the graphite structure. This process is partially reversible, as there is a small anodic peak detectable at c. 1.1 V. Subsequently, a small peak of Li$^+$ intercalation and deintercalation was observed at around 0.25–0.1 V. Aurbach and co-workers [26] studied the intercalation of PP_{13}^+ and Li$^+$ ions using cyclic voltammetry and in situ Raman spectroscopy. In the case of $PP_{13}TFSI$, no anodic peaks were observed, which was contrary to our observations. Besides the intercalation of PP_{13}^+ between the graphene layers, a decomposition mechanism of PP_{13}^+ into radical intermediates was proposed.

This difference can be explained by the presence of lithium cations appearing in the electrolyte from the lithium counter electrode, which may be slightly oxidised during the measurement and the Li$^+$ cations can co-intercalate even during the first cycle (see Fig. 3a). In the subsequent scans, the Li$^+$ deintercalation peak increases together with the decrease of PP_{13}^+ intercalation and deintercalation. Hence, a ternary intercalation compound $Li_x(PP_{13})_yC_z$ is probably formed with a progressive change in composition during cycling [26].

The electrochemical behaviour of the LiTFSI–$PP_{13}TFSI$ electrolyte (Fig. 3b) shows a similar irreversible reduction peak appearing below 0.8 V vs. Li/Li$^+$, similar to the neat ionic liquid system. The peaks of Li$^+$ intercalation and deintercalation are fading with further cycling. In agreement with literature [29] and with our previous observations [34], the TFSI-based electrolyte without a SEI forming agent is not compatible with graphite. This observation was confirmed by the galvanostatic measurements (see Section 3.5).

When LiFSI was used as an electrolyte component, the behaviour of the graphite was different (Fig. 3c). The irreversible reduction occurred in the potential region from 1.3 to 0.25 V, followed by a reversible lithium intercalation into graphite below 0.2 V. Such desirable, reversible behaviour was due to the electrochemical reduction of the FSI^- anion to possible anion-conductive polymer $FSO_2(NSOF)_nN^{(-)}SO_2F$ during the first cycle (so called ionic liquid-based SEI). Cyclic voltammetry illustrates that the film formation was completed during the first cycle. In the second and consequent cycles, no electrochemical reduction was visible any more, indicating that the filming process was completed.

3.4. Galvanostatic measurements in Li/graphite half-cells

The galvanostatic measurements of graphite composite electrodes were performed at 55 °C with the current density

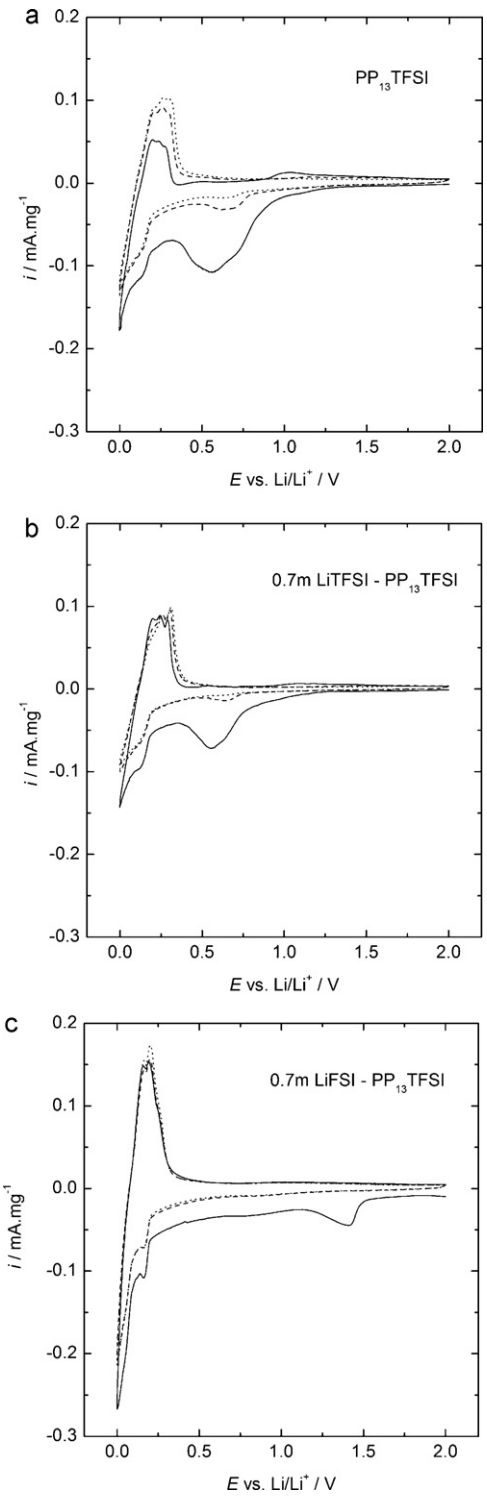

Fig. 3. Initial cyclic voltammograms of a KS6L graphite composite electrode in (a) neat $PP_{13}TFSI$, (b) 0.7m LiTFSI–$PP_{13}TFSI$ and (c) 0.7m LiFSI–$PP_{13}TFSI$ (cycle 1: full line, cycle 2: dash line, cycle 3: dot line). Conditions: 0.1 mV s^{-1}, 55 °C, counter and reference metal lithium.

corresponding to the C/10 rate. The initial three charge–discharge cycles of the Li/KS6L graphite cell with the LiTFSI–$PP_{13}TFSI$ and LiFSI–$PP_{13}TFSI$ electrolytes are given in Fig. 4.

During the first charge of graphite in the LiTFSI–$PP_{13}TFSI$ electrolyte, there was a plateau corresponding to c. 50 mAh g^{-1} at around 0.6 V, which can be ascribed to an irreversible intercalation of the PP_{13}^+ cations into graphite as shown on the cyclic

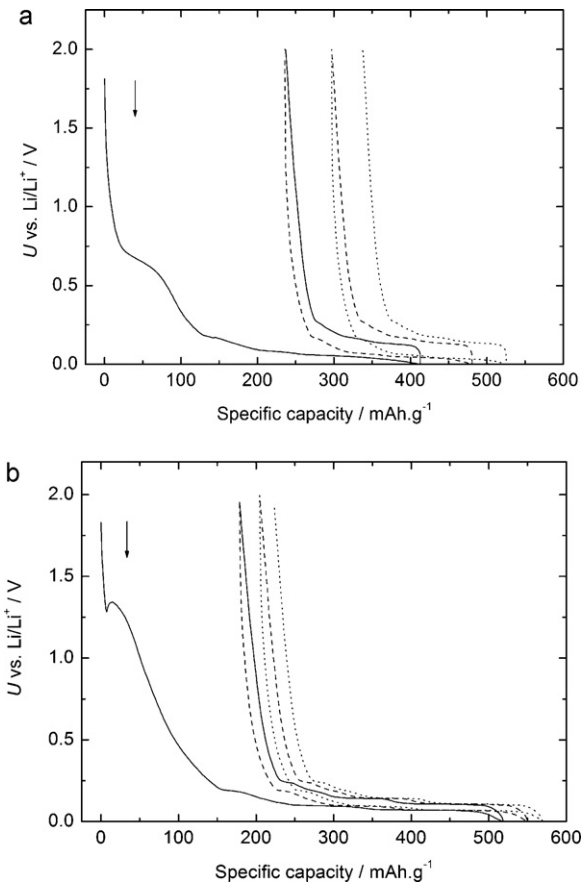

Fig. 4. The initial discharge–charge profiles of the half-cell Li | graphite KS6L in (a) 0.7m LiTFSI–PP_{13}TFSI and (b) 0.7m LiFSI–PP_{13}TFSI electrolyte. Conditions: 55 °C, current density corresponding to C/10.

voltammogram in Fig. 3b. Subsequently, the intercalation of Li^+ was observed between 0.2 and 0 V with the capacity of 280 mAh g^{-1}. The discharge capacity was 177 mAh g^{-1} and no plateau corresponding to the deintercalation of PP_{13}^+ was observed. The overall coulombic efficiency in the first three cycles was 43, 75 and 82%, respectively. The discharge capacity of the half-cell with LiTFSI–PP_{13}TFSI was fading within 10 cycles from 177 to 46 mAh g^{-1} (not shown). This result showed an unstable electrochemical environment for lithium intercalation in graphite when the LiTFSI–PP_{13}TFSI electrolyte was used.

The presence of LiFSI instead of LiTFSI allows the formation of a stable protective SEI, that is an electron insulating and lithium ion conducting film. The onset of SEI formation during the first cycle is consistent with the cathodic peak and wave position obtained in Fig. 3c. After the mild reduction decomposition of the FSI^- anion, the cell voltage rapidly dropped in the voltage region of lithium intercalation into graphite. The discharge capacities and coulombic efficiencies achieved during the first three cycles are summarised in Table 2. As can be seen, the coulombic efficiencies in the first

Table 2
Discharge capacities and coulombic efficiencies for the first three charge–discharge cycles at C/10 rate and 55 °C for KS6L graphite and LiNMC (0.7m LiFSI–PP_{13}TFSI electrolyte).

Electrode material	Discharge capacity (mAh g^{-1})			Coulombic efficiency (%)		
	1st	2nd	3rd	1st	2nd	3rd
KS6L graphite	340	345	346	65.6	93.0	94.9
$LiCo_{1/3}Mn_{1/3}Ni_{1/3}O_2$	169	167	164	92.4	97.8	98.0

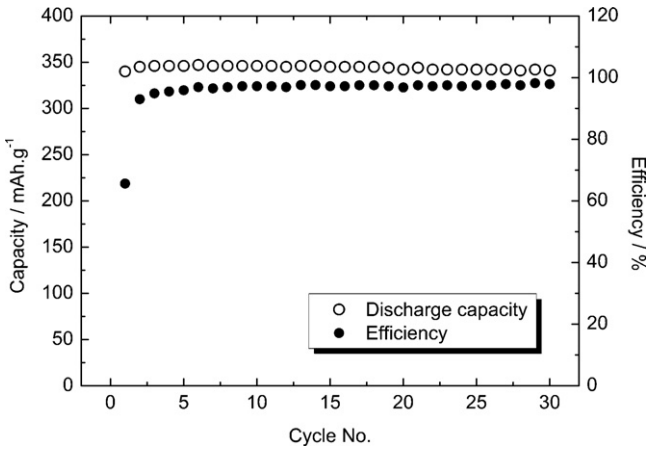

Fig. 5. The cycle performance of KS6L graphite composite electrode in the 0.7m LiFSI–PP_{13}TFSI electrolyte at 55 °C with the current density corresponding to C/10.

three cycles are 65.6, 93.0, and 94.9%. During further cycling, the efficiency soon reaches a stable value of 97–98%.

KS6L graphite showed a good cycling stability (Fig. 5) in the 0.7m LiFSI–PP_{13}TFSI electrolyte, achieving the capacity of 340–345 mAh g^{-1} and with efficiency close to 1.

3.5. Galvanostatic measurements in the Li/NMC half-cells

The charge–discharge performance of Li/NMC cells is presented in Fig. 6. After formation cycles the discharge capacity is stabilised close to 160 mAh g^{-1} with a high cycling efficiency being more than 99%.

By comparing charge–discharge curves in 1st, 5th, and 25th cycle we were not able to observe any remarkable increase of polarisation due to film formation or any other sporadic reaction that are leading to electrode degradation (Fig. 7).

The discharge capacities and coulombic efficiencies achieved during the first three cycles for graphite and NMC are summarised in Table 2.

The presented electrochemical stability of graphite and NMC in the LiFSI–PP_{13}TFSI electrolyte indicates the possibility of using ionic liquid-based electrolytes in full battery cells. Thus the given results can be an excellent starting point for battery engineers to build graphite | LiFSI–PP_{13}TFSI | $LiCo_{1/3}Mn_{1/3}Ni_{1/3}O_2$ cells with novel characteristics leading most probably also to improved safety. This needs to be addressed together with a question about the price of proposed system in the future.

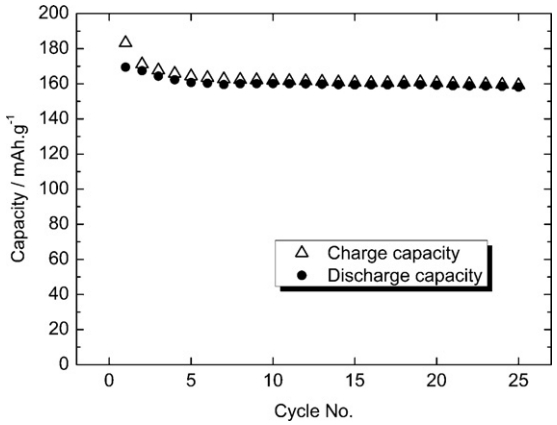

Fig. 6. The charge/discharge capacity of NMC composite electrode in the 0.7m LiFSI–PP_{13}TFSI electrolyte at 55 °C with the current density corresponding to C/10.

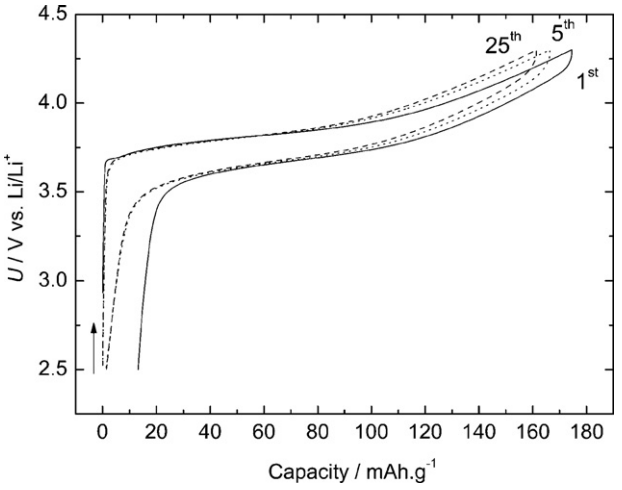

Fig. 7. Comparison of 1st, 5th, and 25th charge/discharge profiles of the half-cell Li | 0.7m LiFSI–PP_{13}TFSI | $LiCo_{1/3}Mn_{1/3}Ni_{1/3}O_2$ at 55 °C with the current density corresponding to C/10.

4. Conclusions

In this paper we have reported the results obtained by using the LiFSI–PP_{13}TFSI electrolyte in combination with KS6L graphite and $LiCo_{1/3}Mn_{1/3}Ni_{1/3}O_2$ at an elevated temperature of 55 °C. The 0.7m LiFSI solution in PP_{13}TFSI exhibits a good ionic conductivity (2.6 mS cm^{-1} at 55 °C), nonflammability and high thermal stability (up to 285 °C).

The use of LiFSI–PP_{13}TFSI showed the high electrochemical stability of the ionic liquid during lithium intercalation into graphite due to the ability of the FSI^- anion to establish the SEI in the formation cycles. This layer is highly conductive to Li^+ cations but prevents further electrolyte degradation. In combination with KS6L graphite, the system studied shows high performance in terms of specific capacity (340–345 mAh g^{-1}) and cycling efficiency (97–98%).

The electrolyte was successfully tested for a representative of the high-voltage cathode material $LiCo_{1/3}Mn_{1/3}Ni_{1/3}O_2$. Electrochemical stability of the electrolyte allows cycling of $LiCo_{1/3}Mn_{1/3}Ni_{1/3}O_2$ in the potential range from 2.5 to 4.3 V and $LiCo_{1/3}Mn_{1/3}Ni_{1/3}O_2$ delivers a capacity of 160 mAh g^{-1} at C/10, respectively. An efficient cycling of $LiCo_{1/3}Mn_{1/3}Ni_{1/3}O_2$ also concludes a good compatibility of LiFSI–PP_{13}TFSI electrolyte with the aluminium current collector at 55 °C at high potentials. The main advantage of the electrolyte is in the absence of volatile additives and the relatively low viscosity of the electrolyte compared to previously studied systems. The SEI-forming agent, FSI anion is an inherent component of the electrolyte.

Acknowledgements

We acknowledge the financial support of the Ministry of Education, Youth and Sports, Czech Republic (LC523), the Grant Agency of the Academy of Sciences of the Czech Republic (KJB200320801 and KJB200320901), the Ministry of Education, Science and Sport of Slovenia, the Slovenian Research Agency and the CO-NOT centre of excellence.

References

[1] M. Armand, F. Endres, D.R. MacFarlane, H. Ohno, B. Scrosati, Nat. Mater. 8 (2009) 621–629.
[2] A. Lewandowski, A. Świderska-Mocek, J. Power Sources 194 (2009) 601–609.
[3] S. Randström, M. Montanino, G.B. Appetecchi, C. Lagergren, A. Moreno, S. Passerini, Electrochim. Acta 53 (2008) 6397–6401.
[4] G.B. Appetecchi, M. Montanino, D. Zane, M. Carewska, F. Alessandrini, S. Passerini, Electrochim. Acta 54 (2009) 1325–1332.
[5] A. Guerfi, S. Duchesne, Y. Kobayashi, A. Vijh, K. Zaghib, J. Power Sources 175 (2008) 866–873.
[6] A. Lewandowski, A.F. Hollenkamp, S.W. Donne, A.S. Best, J. Power Sources 195 (2010) 2029–2035.
[7] Y. Abu-Lebdeh, A. Abouimrane, P.-J. Alarco, M. Armand, J. Power Sources 154 (2006) 255–261.
[8] S. Fang, Z. Zhang, Y. Jin, L. Yang, S.-I. Hirano, K. Tachibana, S. Katayama, J. Power Sources 196 (2011) 5637–5644.
[9] M. Nadherna, R. Dominko, D. Hanzel, J. Reiter, M. Gaberscek, J. Electrochem. Soc. 156 (2009) A619–A626.
[10] H. Zheng, B. Li, Y. Fu, T. Abe, Z. Ogumi, Electrochim. Acta 52 (2006) 1556–1562.
[11] H. Zheng, H. Zhang, Y. Fu, T. Abe, Z. Ogumi, J. Phys. Chem. B 109 (2005) 13676–13684.
[12] E. Markevich, V. Baranchugov, D. Aurbach, Electrochem. Commun. 8 (2006) 1331–1334.
[13] V. Borgel, E. Markevich, D. Aurbach, G. Semrau, M. Schmidt, J. Power Sources 189 (2009) 331–336.
[14] J. Mun, T. Yim, K. Park, J.H. Ryu, Y.G. Kim, S.M. Oh, J. Electrochem. Soc. 158 (2011) 454–457.
[15] J. Saint, A.S. Best, A.F. Hollenkamp, J. Kerr, J.-H. Shin, M.M. Doeff, J. Electrochem. Soc. 155 (2008) A172–A180.
[16] H. Sakaebe, H. Matsumoto, Electrochem. Commun. 5 (2003) 594–598.
[17] B. Garcia, S. Lavallér, G. Perron, Ch. Michot, M. Armand, Electrochim. Acta 49 (2004) 4583–4588.
[18] M. Holzapfel, C. Jost, A. Prodi-Schwab, F. Krumeich, A. Würsig, H. Buqa, P. Novák, Carbon 43 (2005) 1488–1498.
[19] H. Sakaebe, H. Matsumoto, K. Tatsumi, J. Power Sources 146 (2005) 693–697.
[20] H. Matsumoto, H. Sakaebe, K. Tatsumi, M. Kikuta, E. Ishiko, M. Kono, J. Power Sources 160 (2006) 1308–1313.
[21] M. Egashira, M. Tanaka-Nakagawa, I. Watanabe, S. Okada, J.I. Yamaki, J. Power Sources 160 (2006) 1387–1390.
[22] S. Seki, Y. Ohno, Y. Kobayashi, H. Miyashiro, A. Usami, Y. Mita, H. Tokuda, M. Watanabe, K. Hayamizu, S. Tsuzuki, J. Electrochem. Soc. 154 (2007) A173–A177.
[23] N.S. Choi, Y. Lee, S.S. Kim, S.C. Shin, Y.M. Kang, J. Power Sources 195 (2010) 2368–2371.
[24] H. Zheng, K. Jiang, T. Abe, Z. Ogumi, Carbon 44 (2006) 203–210.
[25] X.-G. Sun, S. Dai, Electrochim. Acta 55 (2010) 4618–4626.
[26] E. Markevich, V. Baranchugov, G. Salitra, D. Aurbach, M.A. Schmidt, J. Electrochem. Soc. 155 (2008) A132–A137.
[27] A. Lewandowski, A. Świderska-Mocek, J. Power Sources 194 (2009) 502–507.
[28] I.A. Profatilova, N.-S. Choi, S.W. Roh, S.S. Kim, J. Power Sources 192 (2009) 636–643.
[29] G.B. Appetecchi, M. Montanino, A. Balducci, S.F. Lux, M. Winter, S. Passerini, J. Power Sources 192 (2009) 599–605.
[30] S.F. Lux, M. Schnuck, G.B. Appetecchi, S. Passerini, M. Winter, A. Balducci, J. Power Sources 192 (2009) 606–611.
[31] T. Sugimoto, Y. Atsumi, M. Kikuta, E. Ishiko, M. Kono, M. Ishikawa, J. Power Sources 189 (2009) 802–805.
[32] E. Paillard, Q. Zhou, W.A. Henderson, G.B. Appetecchi, M. Montanino, S. Passerini, J. Electrochem. Soc. 156 (2009) A891–A895.
[33] Y.D. Wang, K. Zaghib, A. Guerfi, F.F.C. Bazito, R.M. Torresi, J.R. Dahn, Electrochim. Acta 52 (2007) 6346–6352.
[34] M. Nadherna, J. Reiter, J. Moskon, R. Dominko, J. Power Sources 196 (2011) 7700–7706.
[35] L. Larush, V. Borgel, E. Markevich, O. Haik, E. Zinigrad, D. Aurbach, G. Semrau, M. Schmidt, J. Power Sources 189 (2009) 217–223.
[36] C. Arbizzani, G. Gabrielli, M. Mastragostino, J. Power Sources 196 (2011) 481–4805.
[37] H.F. Xiang, B. Yin, H. Wang, H.W. Lin, X.W. Ge, S. Xie, C.H. Chen, Electrochim. Acta 55 (2010) 5204–5209.
[38] H.B. Han, S.S. Zhou, D.J. Zhang, S.W. Feng, L.F. Li, K. Liu, W.F. Feng, J. Nie, H. Li, X.J. Huang, M. Armand, Z.B. Zhou, J. Power Sources 196 (2011) 3623–3632.
[39] A. Abouimrane, J. Ding, I.J. Davidson, J. Power Sources 189 (2009) 693–696.
[40] Q. Zhou, W.A. Henderson, G.B. Appetecchi, M. Montanino, S. Passerini, J. Phys. Chem. 112 (2008) 13577–13580.
[41] M. Beran, J. Příhoda, Z. Anorg, Allg. Chem. 631 (2005) 55–59.
[42] M. Beran, J. Příhoda, Z. Žák, M. Černík, Polyhedron 25 (2006) 1292–1298.
[43] R.S. Kühnel, N. Böckenfeld, S. Passerini, M. Winter, A. Balducci, Electrochim. Acta 56 (2011) 4092–4099.
[44] A. Chagnes, M. Diaw, B. Carré, P. Willmann, D. Lemordant, J. Power Sources 145 (2005) 82–88.
[45] G.B. Appetecchi, M. Montanino, M. Carewska, F. Alessandrini, S. Passerini, Adv. Sci. Technol. 72 (2010) 315–319.
[46] H.S. Choe, B.G. Carroll, D.M. Pasquariello, K.M. Abraham, Chem. Mater. 9 (1997) 369–379.